Improved discovery of a nearly degenerate model: Minimal universal extra dimension model using M_{T2} at the LHC

Hitoshi Murayama, Mihoko M. Nojiri, and Kohsaku Tobioka

Phys. Rev. D **84**, 094015 — Published 14 November 2011
DOI: 10.1103/PhysRevD.84.094015

IPMU11-0104

Improved discovery of nearly degenerate model: MUED using M_{T2} at the LHC

Hitoshi Murayama[a,b], Mihoko Nojiri[b,c], and Kohsaku Tobioka[b,d]

[a] *Department of Physics, University of California, Berkley CA94720*
Theoretical Physics Group, Lawrence Berkley National Laboratory, Berkley CA94720

[b] *Institute for the Physics and Mathematics of the Universe,*
University of Tokyo, Kashiwa 277-8583, Japan

[c] *Theory Group, KEK, Tsukuba 305-0801, Japan*
The Graduate University for Advanced Studies (Sokendai), Tsukuba 305-0801, Japan

[d] *Department of Physics, University of Tokyo, Tokyo 113-0033, Japan*

Abstract

We study the discovery potential of the Minimal Universal Extra Dimension model (MUED) and improve it utilizing the multijet + lepton mode at the LHC. Since the MUED has a nearly degenerate spectrum, most events only have soft jets and small E_T^{miss}. The signature is challenging to search. We apply M_{T2} for the event selection and set the invisible particle mass of M_{T2} (test mass) to zero. The test mass is much smaller than the invisible particle mass of MUED. In that case, M_{T2} of the signal can be large depending on Up-Stream Radiations (USR) which includes initial state radiations (ISR). On the other hand, M_{T2} of the background is mainly below the top quark mass. Hence, the signal is extracted from the background in the high M_{T2} region. Since we use the leading jets for M_{T2}, there is a combinatorics effect. We found the effect also enhances the signal to background ratio for high M_{T2}. We perform a detailed simulation with the Matrix Element correction to the QCD radiations. The discovery potential of the MUED is improved by the M_{T2} cut, and especially, the improvement is significant for the most degenerate parameter we consider, $\Lambda R = 10$.

1 Introduction

In the last decade, extra dimensional models were studied as possible extensions of the Standard Model (SM). The Universal Extra Dimensions model (UED) was developed by Appelquist, Cheng, and Dobrescu [1] (see [2] for review). While other types of extra dimension like the ADD model [3] and the RS model [4] are meant to solve the gauge hierarchy problem, the UED is motivated by the Dark Matter problem [5]. One of the most attractive ways to explain Dark Matter is a new weakly interacting particle (WIMP), and the UED contains WIMP.

In the UED, all the SM fields propagate in the flat extra dimensions. The fields are expanded in discrete Kaluza-Klein (KK) modes called KK particles according to the KK number, the extra dimensional momentum, in the 4D effective theory. In the 5D UED, the extra dimension is compactified on an S^1/Z_2 orbifold to obtain the SM chiral fermions in the zero mode. This orbifold violates momentum conservation in the extra dimension but KK parity remains unbroken. KK number odd (even) modes have odd (even) KK parity, and the SM particles have the even KK parity. The lightest KK odd particle (LKP) is stable because this cannot decay into the SM particles due to the KK parity.

We consider the Minimal Universal Extra Dimension model (MUED). The mass spectrum of each KK level at the tree-level is highly degenerate in mass: mass of the nth KK level is approximately n/R, where R is the radius of the compactified extra dimension. The degeneracy is a little relaxed due to radiative corrections at the one-loop level [6, 7]. The contribution of the radiative corrections is large when ΛR is large, where Λ is a cutoff scale of the MUED. However, ΛR cannot be larger than $\Lambda R \sim 40$, because the running gauge coupling of $U(1)_Y$ increases as power law beyond the MUED scale $1/R$ and blows up at $\sim 40/R$. So the mass spectrum is still nearly degenerate.

For most choices of parameters, LKP is the first KK photon $\gamma^{(1)}$ which is a good Dark Matter candidate. In calculating the relic abundance of LKP $\gamma^{(1)}$ in the nearly degenerate spectrum, the co-annihilation effect takes an important role [5, 8, 9]. The second KK particles also enter in the computation at the one loop level [10, 11, 12]. The mass scale of LKP Dark Matter consistent with the cosmological observations is $1/R \sim 1.5$ TeV [12].

The collider signature of the model with the nearly degenerate spectrum is more difficult to find because produced visible particles tend to be soft [13]. The well-studied new physics model is Supersymmetry (SUSY) with large mass splittings, and the decay of the colored SUSY particles produces hard jets and large E_T^{miss}. However, in the MUED, soft jets and small E_T^{miss} are mostly generated due to the spectrum.

The discovery studies at Hadron Colliders have been carried out since the MUED was proposed [14, 15, 16, 17, 18]. Previous studies were mainly based on the multilepton channels [14, 16, 17, 18] and the most promising one is $4l + E_T^{miss}$ in which the background level is quite low [14, 16, 17]. But the signal events remain very small in this analysis because this channel is accessible to very limited production processes of MUED. The analysis including background systematic uncertainties was studied by the CMS collaboration [16], and the discovery reach is $1/R \sim 600$ GeV with 1 fb^{-1} at $\sqrt{s} = 14$ TeV. Since the LKP dark matter scenario favors the very high mass scale $m_{LKP} \cong 1/R \sim 1.5$ TeV [12], it is challenging to look for the signature in $4l + E_T^{miss}$. In order to check the scenario at the LHC, the sensitivity should be improved, and therefore, we need an alternative way to search for the MUED.

Multijet channels without requiring multilepton have a statistical advantage because most MUED events have multiple jets, even though the analysis based on hard jets and large E_T^{miss} cannot deal with the signal of the nearly degenerate model due to the softness of jets and small E_T^{miss}. The problem of the ordinary multijet $+E_T^{miss}$ analysis is that the signal is buried in the SM background. This is because the top quark pair production $t\bar{t}$ generates missing particles, neutrinos, and hard jets with a large enough cross section. If there exists a method that can extract the signal from the background based on jets, the discovery potential of the MUED could be improved.

We tackle the search in the multijet channel by using a kinematic variable M_{T2} [19, 20], sometimes called "Stransverse Mass". M_{T2} was originally proposed to measure masses of pair-produced particles in the situation with two invisible particles. When the true mass of invisible particle is given, M_{T2} is bounded by the mass of the produced particles. It was proposed that M_{T2} can be used not only as a mass measurement variable but for the event selection [21, 22], and this has been applied for the SUSY search by the ATLAS [23] and CMS [24] Collaborations.

In this paper, we point out that M_{T2} is effective for the search of the nearly degenerate model like the MUED. To use M_{T2} as an event selection, we need to set a test mass for the invisible particle, and it is set to zero. The set test mass is wrong for the MUED events because it is much smaller than the mass of LKP. This leads to the M_{T2} dependence on Up-Stream Radiations (USR). USR is defined as visible particles which contribute to the recoil momentum of the subsystem of the pair-produced particles, and they are mainly initial state radiations (ISR). M_{T2} of the signal can be large depending on USR, although, without USR, M_{T2} is small in the nearly degenerate spectrum. On the other hand, the test mass is correct for the mass of the SM invisible particle, neutrino. Then, M_{T2} of the SM background does not depend on USR. As shown in Refs. [19, 20], it is mainly below the mass of the heaviest particle in the SM, the top quark, $M_{T2}^{\rm SM} \lesssim m_{top}$. Therefore, an excess in the high M_{T2} region beyond m_{top} can be seen as the signal of a nearly degenerate model, and then, M_{T2} is effective to search for the MUED.

In the analysis of this paper, leading two jets in p_T are used to calculate M_{T2}. They do not always correspond to jets we want, that is, we have combinatoric issues when choosing jets for defining M_{T2}. Combinatorics smears the M_{T2} distribution, and the smearing effect is different in each process. We found combinatorics makes M_{T2} of the signal larger while M_{T2} of the background does not increase as much as that of the signal. Therefore, the smearing effect of combinatorics enhances the signal excess in the high M_{T2} region.

We apply M_{T2} to the discovery study of the MUED, and we require at least one lepton in addition to multijet to avoid the QCD background. Since the ISR takes an important role in this method, we perform the event generation with the Matrix Element correction which evaluates the hard ISR appropriately. This way, we show that the M_{T2} analysis improves the discovery potential compared to the $4l + E_T^{miss}$ analysis.

The paper is organized as follows: in section 2 we briefly review the MUED and describe its LHC signature, the relic abundance of the LKP, and the experimental constraints. In section 3, we discuss M_{T2} for the event selection in searching for the MUED signal. The simulation setup is presented in section 4. We present our analysis result and show that the discovery potential of the MUED is improved in section 5. Section 6 contains discussion and conclusion.

2 The Minimal Universal Extra Dimension model

2.1 Setup

In the case of the 5D UED, there is a compactified flat extra dimension in which all the SM fields universally propagate in addition to the 4D Minkowski space-time. Fields are expanded in the KK modes (KK particles) in the 4D effective theory, and each zero mode corresponds to the SM particle. For example, the 5D real scalar field is decomposed in an infinite number of the KK modes after integration of the compactified extra dimension y,

$$\int d^4x \int_{-\pi R}^{\pi R} dy \quad \Phi(x,y) \left(\partial^2 - \partial_5^2 - m_{SM}^2\right) \Phi(x,y) \tag{1}$$

$$= \int d^4x \sum_{n=-\infty}^{\infty} \phi^{(-n)}(x) \left(\partial^2 - \left\{ \left(\frac{n}{R}\right)^2 + m_{SM}^2 \right\}\right) \phi^{(n)}(x) \tag{2}$$

$$= \int d^4x \sum_{n=-\infty}^{\infty} \phi^{(-n)}(x) \left(\partial^2 - m_n^2\right) \phi^{(n)}(x) \tag{3}$$

where

$$\Phi(x,y) = \frac{1}{\sqrt{2\pi R}} \sum_{n=-\infty}^{\infty} \phi^{(n)}(x) e^{i\frac{n}{R}y} \tag{4}$$

and $m_n^2 = m_{SM}^2 + (n/R)^2$. R denotes the radius of the extra dimension, and m_{SM} denotes a SM particle mass. The fifth dimensional momentum is the mass in the 4D effective theory, and this is much greater than m_{SM}, because $1/R \sim O(\text{TeV})$. Therefore, we can neglect m_{SM}: $m_n \simeq n/R$, which means the mass spectrum of each KK level is highly degenerate.

Since the simple compactified extra dimension S^1 gives vector-like fermions, an orbifold compactified extra dimension S^1/Z_2 with an identification of $y \leftrightarrow -y$ is considered in order to obtain chiral fermions in the zero mode. The orbifold compactification results in another significant characteristic, the KK parity. KK number is conserved by virtue of the fifth dimensional momentum conservation on S^1 compactification, but this is broken down to the KK parity by the orbifold compactification. The KK parity reflects "evenness" and "oddness" of the KK number. All the SM particles have the even KK parity. The lightest particle with the odd KK parity, called the lightest Kaluza-Klein particle (LKP), is stable since it cannot decay into lighter SM particles due to its oddness. The stable LKP, typically the first KK photon $\gamma^{(1)}$, can be a weakly interacting massive particle (WIMP) and therefore a good Dark Matter candidate.

To discuss collider phenomenology, we have to determine the mass spectrum. In this paper, we discuss the Minimal Universal Extra Dimenison model (MUED). The MUED is a minimal extension of the 4D SM Lagrangian to the 5D UED. At the cutoff scale Λ it contains only SM fields and no other terms, especially no localized terms at two fixed points $y = 0, \pi R$ led by orbifold compactification. The model parameters of MUED are only three: 5D radius R, cutoff scale of MUED Λ, and the SM Higgs mass m_h.

2.2 Mass spectrum

Radiative corrections to masses of the KK modes at the one-loop level were studied in Refs. [6, 7]. This correction enlarges mass splitting for each KK level away from the highly degenerate mass spectrum. The corrected masses are:

$$\begin{aligned} m_{X^{(n)}}^2 &= \frac{n^2}{R^2} + m_{X^{(0)}}^2 + \delta m_{X^{(n)}}^2 \quad \text{(Boson)}, \\ m_{X^{(n)}} &= \frac{n}{R} + m_{X^{(0)}} + \delta m_{X^{(n)}} \quad \text{(Fermion)}, \end{aligned} \tag{5}$$

where $m_{X^{(0)}}$ is a SM particle (zero mode) mass. Since $1/R$ is taken to be larger than 400 GeV as mentioned in Sec. 2.4, $m_{X^{(0)}}$ is much smaller than $1/R$. The neutral gauge bosons of $U(1)_Y$

and $SU(2)_L$ are mixed up in the SM, but mass eigenstates of the KK neutral gauge bosons, $\gamma^{(n)}$ and $Z^{(n)}$, are nearly $U(1)_Y$ and $SU(2)_L$ gauge eigenstates, $B^{(n)}$ and $W^{3(n)}$, respectively because the diagonal components of mass matrix dominates as

$$\begin{pmatrix} B^{(n)} & W^{3(n)} \end{pmatrix} \begin{pmatrix} \frac{n^2}{R^2} + \delta m^2_{B^{(n)}} + \frac{1}{4}g'^2 v^2 & \frac{1}{4}g' g v^2 \\ \frac{1}{4}g' g v^2 & \frac{n^2}{R^2} + \delta m^2_{W^{3(n)}} + \frac{1}{4}g^2 v^2 \end{pmatrix} \begin{pmatrix} B^{(n)} \\ W^{3(n)} \end{pmatrix} \tag{6}$$

where g' is the gauge coupling of $U(1)_Y$, g is that of $SU(2)_L$, and $v = 246$ GeV is the vacuum expectation value of the Higgs field. The radiative corrections to gauge boson masses are given by

$$\begin{aligned} \delta m^2_{B^{(n)}} &= -\frac{39}{2}\frac{g'^2\zeta(3)}{16\pi^2}\frac{1}{R^2} + \frac{n^2}{R^2}\left(-\frac{1}{6}\frac{g'^2}{16\pi^2}\right)\ln(\Lambda R)^2 \\ \delta m^2_{W^{(n)}} &= -\frac{5}{2}\frac{g^2\zeta(3)}{16\pi^2}\frac{1}{R^2} + \frac{n^2}{R^2}\left(\frac{15}{2}\frac{g^2}{16\pi^2}\right)\ln(\Lambda R)^2 \\ \delta m^2_{g^{(n)}} &= -\frac{3}{2}\frac{g_s^3\zeta(3)}{16\pi^2}\frac{1}{R^2} + \frac{n^2}{R^2}\left(\frac{23}{2}\frac{g_s^2}{16\pi^2}\right)\ln(\Lambda R)^2 \end{aligned} \tag{7}$$

where $\zeta(3) = 1.20205...$ and g_s is the gauge coupling of $SU(3)_C$. The second terms in the corrections are dominant, so $m_{W^{(n)}}$ is lifted, and $m_{B^{(n)}}$ is slightly lowered.

The mixings of the KK quarks (KK leptons) are also negligible, and they become $U(1)_Y$ and $SU(2)_L$ gauge eigenstates. Neglecting m_{SM}, radiative corrections to the KK quarks and KK leptons are given by

$$\begin{aligned} \delta m_{Q^{(n)}} &= \frac{n}{R}\left(3\frac{g_s^2}{16\pi^2} + \frac{27}{16}\frac{g^2}{16\pi^2} + \frac{1}{16}\frac{g'^2}{16\pi^2}\right)\ln(\Lambda R)^2 \\ \delta m_{u^{(n)}} &= \frac{n}{R}\left(3\frac{g_s^2}{16\pi^2} + \frac{g'^2}{16\pi^2}\right)\ln(\Lambda R)^2 \\ \delta m_{d^{(n)}} &= \frac{n}{R}\left(3\frac{g_3^2}{16\pi^2} + \frac{1}{4}\frac{g'^2}{16\pi^2}\right)\ln(\Lambda R)^2 \\ \delta m_{L^{(n)}} &= \frac{n}{R}\left(\frac{27}{16}\frac{g^2}{16\pi^2} + \frac{9}{16}\frac{g'^2}{16\pi^2}\right)\ln(\Lambda R)^2 \\ \delta m_{e^{(n)}} &= \frac{n}{R}\left(\frac{9}{4}\frac{g'^2}{16\pi^2}\right)\ln(\Lambda R)^2 \end{aligned} \tag{8}$$

where $Q^{(n)}$ and $L^{(n)}$ denote the $SU(2)_L$ doublet, and $u^{(n)}$, $d^{(n)}$, and $e^{(n)}$ denote the $SU(2)_L$ singlet. For the KK top quark we should consider the correction from its Yukawa coupling, but the production cross section is small. We do not consider the processes of KK top quark.

Most KK particles receive positive mass corrections. The heaviest particle in each level is $g^{(n)}$ for the largest correction, and the lightest particle in each level is typically $\gamma^{(n)}$. Then the LKP is $\gamma^{(1)}$ with the mass $m_{\gamma^{(1)}} \cong 1/R$. If the Higgs boson of the SM is as heavy as $m_h \gtrsim 240$ GeV, the first KK charged Higgs $h^{\pm(1)}$ can be LKP due to the negative mass correction of the Higgs four point coupling. But, of course, this cannot be the Dark Matter. In this paper, we fix the Higgs mass at $m_h = 120$ GeV, and we keep $\gamma^{(1)}$ as LKP so that it is the Dark Matter candidate.

The corrections are basically proportional to $\ln \Lambda R$, so the degeneracy is crucial for the smaller ΛR. The cutoff scale of the UED was discussed in [25], and the appropriate cutoff scale should be several dozen $1/R$ for a given R. As the energy scale grows, more KK particles appear, and the logarithmic running of the gauge coupling changes into power law running above the MUED scale $1/R$. The $U(1)_Y$ gauge coupling blows up (Landau pole) at the energy scale $\sim 40/R$, so we should set the cutoff scale below the Landau pole. The very small ΛR is also not appropriate because we should consider the higher dimensional operators, and the MUED framework is not a good effective theory any more. In our analysis, we considered $10 \leq \Lambda R \leq 40$. A benchmark point of MUED is chosen as $1/R = 800$ GeV, $\Lambda R = 20$, and table 1 shows its mass spectrum.

$m_{\gamma^{(1)}}$	$m_{W^{(1)}}$	$m_{Z^{(1)}}$	$m_{e^{(1)}}$	$m_{L^{(1)}}$	$m_{d^{(1)}}$	$m_{u^{(1)}}$	$m_{Q^{(1)}}$	$m_{g^{(1)}}$	
800.1	847.3	847.4	808.2	822.3	909.8	912.5	929.3	986.4	GeV

Table 1: Mass spectrum of first KK level for a benchmark point $(1/R, \Lambda R) = (800, 20)$

2.3 Production and decay at the LHC

At the LHC, the first KK particles of the odd KK parity are pair-produced, and they eventually decay into the LKP. The dominant production processes are KK gluon+KK quark ($g^{(1)} + Q^{(1)}/q^{(1)}$) and KK quark+KK quark ($Q^{(1)}/q^{(1)} + Q^{(1)}/q^{(1)}$). The cross sections of the colored particles are shown in [15]. For our benchmark point, $\sigma(g^{(1)}+Q^{(1)}/q^{(1)}) = 12.2$ pb and $\sigma(Q^{(1)}/q^{(1)} + Q^{(1)}/q^{(1)}) = 7.4$ pb at $\sqrt{s} = 14$ TeV. The $g^{(1)}$ decays into $Q^{(1)}Q$ and $q^{(1)}q$ with branching ratios, BR($g \to Q^{(1)}Q$) $\sim 40\%$ and BR($g \to q^{(1)}q$) $\sim 60\%$, respectively. The ratio of inclusive KK quark productions is roughly $Q^{(1)}Q^{(1)} : q^{(1)}q^{(1)} : Q^{(1)}q^{(1)} = 1 : 1 : 2$. Because $q^{(1)}$ only has the $U(1)_Y$ gauge interaction, it directly decays into $\gamma^{(1)}q$. The hard jets mainly come from this decay. The branching ratios of $Q^{(1)}$ are typically BR($Q^{(1)} \to QW^{\pm(1)}$) $\sim 65\%$, BR($Q^{(1)} \to QZ^{(1)}$) $\sim 32\%$, and BR($Q^{(1)} \to Q\gamma^{(1)}$) $\sim 3\%$. Once $W^{(1)}$ and $Z^{(1)}$ appear from $Q^{(1)}$, they cannot decay hadronically for kinematical reasons. They democratically decay into all lepton flavors: $W^{\pm(1)} \to \gamma^{(1)} l\nu$ and $Z^{(1)} \to \gamma^{(1)}\nu\bar{\nu}$ or $\gamma^{(1)}l^+l^-$ through $l^{(1)}$ or $\nu^{(1)}$.

This collider signature has been studied in clean channels of multilepton such as $4l + E_T^{miss}$ [14, 16, 17], dilepton, and trilepton [17, 18]. The missing transverse energy E_T^{miss} is a magnitude of missing transverse momentum $\mathbf{p}_T^{miss}$ which is measured by the negative sum of transverse momenta of visible particles , $\mathbf{p}_T^{miss} = -\sum \mathbf{p}_T^{jet} - \sum \mathbf{p}_T^{lep}$. The leptons arise only from the KK gauge boson $W^{(1)}$ or $Z^{(1)}$ production. The $4l + E_T^{miss}$ channel has been the most promising one because the background is extremely small, but the fraction of the MUED events going to this channel is about 1%: from the $Q^{(1)}Q^{(1)}$ production, each $Q^{(1)}$ should decay as $Q^{(1)} \to QZ^{(1)} \to Ql^+l^-\gamma^{(1)}$ with the branching ratio of 16%.

Multijet channels without requiring multileptons are statistically advantageous, so we use the multijet + lepton channel. This is accessible to about 65% of the MUED total production. The requirement of one lepton is only to avoid the QCD background.

However, we face the difficulty of relativity small p_T^{jet} and E_T^{miss} due to the small mass splitting between produced colored particles and LKP. Then, the ordinary multijet + E_T^{miss} analysis optimized for the typical SUSY expecting hard jets and large E_T^{miss} is not effective for the search for the nearly degenerate model: MUED. It is important to study a way to squarely address the nearly degenerate model using multijet because the discovery potential of the MUED could be improved for the statistical advantage. In order to search the signal of the nearly degenerate model in the channel we choose, we apply M_{T2} to an event selection described in Sec. 3.

2.4 Relic abundance of LKP and experimental constraints

The LKP Dark Matter relic abundance has been studied in Refs. [5, 8, 9, 10, 11, 12]. Inclusion of co-annihilation processes is essential for the correct estimation of the LKP mass. In the co-annihilation calculation, the effect of s-channel resonances of the second KK particles [10, 11] and the effect of the final states with the second KK particles [12] must be considered. The MUED mass scale $1/R$ consistent with cosmological observations is $1/R \sim 1.5$ TeV including these effects [12]. In this case, it is challenging to discover the MUED both at the first run ($\sqrt{s} = 7$ TeV) and at the second run ($\sqrt{s} = 14$ TeV) with a low luminosity $O(1)$ fb^{-1}. Hence, it is important to enhance the discovery potential of the MUED by developing a new technique and/or a new channel to check the LKP Dark Matter scenario at the LHC.

The electroweak precision test suggests the energy scale of the extra dimension $1/R$ should be greater then 550 GeV for $m_h = 100$ GeV and 350 GeV for $m_h = 400$ GeV at the 95% C.L. [26, 27]. Independent of the Higgs mass, the observed branching ratio of $B_d \to X_s\gamma$ constrains $1/R > 600$GeV at the 95% C.L. [28, 29, 30].

We have obtained a collider bound on the MUED from the ATLAS SUSY search in multijet $+E_T^{miss}$ with 35 pb^{-1} [23] and 1 fb^{-1} [31] data and in multijet + one lepton $+E_T^{miss}$ with 1 fb^{-1} data [32]. It gives an upper limit on cross sections after several cuts. We have checked which parameters of MUED are excluded using Monte Carlo samples generated by PYTHIA[33] [1], and we found that $1/R \leq 600$ GeV with $10 \leq \Lambda \leq 40$ is excluded by the multijet $+E_T^{miss}$ analysis [31] at the 95% C.L.

Then, we focus on 400 GeV $\leq 1/R \leq$ 1600 GeV due to the LKP abundance, the branching ratio of $B_d \to X_s\gamma$, the elctroweak precision test, and the LHC constraint.

3 Method for Searching for the MUED

3.1 M_{T2}

Our idea is to apply M_{T2} to the event selection when searching for the MUED. The effectiveness of M_{T2} to search for SUSY were discussed in [21, 22], and M_{T2} was already applied in the search for SUSY in multijet + E_T^{miss} by the ATLAS collaboration [23].

We briefly review the definition of M_{T2}. M_{T2}, an extension of transverse mass M_T, was originally proposed as a mass measurement variable in the situation with two invisible particles [19, 20]. In each event, we only know the total missing transverse momentum, $\mathbf{p}_T^{miss}$, but each transverse momentum of the invisible particle cannot be measured. The definition of M_{T2} is :

$$M_{T2} \equiv \min_{\mathbf{p}_T^{inv(1)}+\mathbf{p}_T^{inv(2)}=\mathbf{p}_T^{miss}} \left[\max\left\{M_T^{(1)},\ M_T^{(2)}\right\}\right] \tag{9}$$

where M_T is defined by

$$\begin{aligned} M_T^{(i)} &= M_T(m_{vis(i)}, m_{inv(i)}, \mathbf{p}_T^{vis(1)}, \mathbf{p}_T^{inv(1)}) \\ &\equiv \sqrt{m_{vis(i)}^2 + m_{inv(i)}^2 + 2\left(E_T^{vis(i)}E_T^{inv(i)} - \mathbf{p}_T^{vis(i)} \cdot \mathbf{p}_T^{inv(i)}\right)}, \end{aligned} \tag{10}$$

The transverse energy E_T is given by

$$E_T \equiv \sqrt{m^2 + |\mathbf{p}_T|^2}. \tag{11}$$

In calculating M_{T2}, we first construct transverse mass $M_T^{(i=1,2)}$ and take the maximum of them for one partition of $\mathbf{p}_T^{inv(1)}$ and $\mathbf{p}_T^{inv(2)}$ satisfying $\mathbf{p}_T^{inv(1)} + \mathbf{p}_T^{inv(2)} = \mathbf{p}_T^{miss}$. Then, all the possible partitions are considered, and the minimum value among them is taken.

[1]The event generation of MUED that was used for this bound is described in Sec. 4.1.

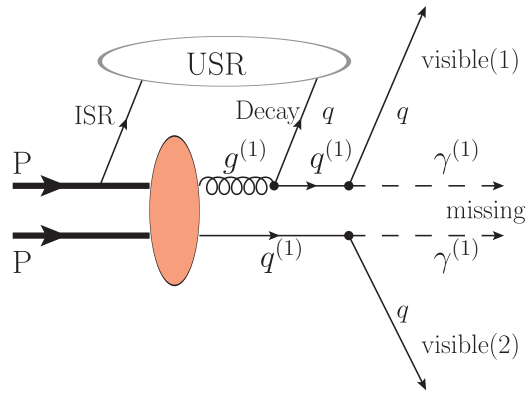

Figure 1: Schematic picture of typical MUED process, $g^{(1)}q^{(1)}$ production. When two jets from $q^{(1)} \to \gamma^{(1)}q$ and used as visible particles to construct M_{T2}, a jet from the decay of $g^{(1)} \to q^{(1)}q$ and ISR become USR.

Let us consider the simple case where the same parent particles are produced and each of them directly decay to a visible particle and an invisible particle. If the invisible particle mass m_{inv} is known, M_T is bounded by the parent particle mass, $M_T \leq m_{parent}$ in the correct partition. Then, as seen from the definition, M_{T2} is also bounded by the parent particle mass, $M_{T2} \leq m_{parent}$. We can also interprete $M_{T2}^{\max}$ as the invariant mass.

In practice, m_{inv} is not known. In calculating M_{T2}, we need to set a test mass for the invisible particle. Many attempts were made to simultaneously determine the masses of the parent and invisible particles [34, 35, 36, 37, 38, 39]. One of them [39] utilizes the effect of Up-stream Radiations (USR). USR is defined as visible particles which are emitted before parent particles of our interest are produced. The transverse momentum of USR, $\mathbf{P}_T$, is given by,

$$\mathbf{p}_T^{vis(1)} + \mathbf{p}_T^{vis(2)} + \mathbf{p}_T^{miss} = -\mathbf{P}_T \quad \text{(USR)}. \tag{12}$$

$\mathbf{P}_T$ is a measure of the recoil of the parent particles. The source of USR is mainly initial state radiations (ISR). The decay products can be USR if the decay is before the production of the parent particles. Fig. 1 illustrates USR in a case of $g^{(1)}q^{(1)}$ production. When we are interested in $q^{(1)}$, a quark emitted from the decay of $g^{(1)}$ and ISR are considered as USR.

Of course, $M_{T2}^{\max}$ has different behaviors depending on whether the test mass is correct. When we set a correct test mass, $M_{T2}^{\max}$ corresponds to the parent particle mass independent of USR. But, when we set a wrong test mass, $M_{T2}^{\max}$ varies with USR. This is because M_T varies with USR and is no longer bounded by the parent particle mass. This property can be used in the search for MUED.

3.2 M_{T2} for the event selection

The features of M_{T2} for the purpose of event selection were studied in [21, 22]. We use the M_{T2} cut as an event selection setting the test mass to zero. The set test mass is a correct value for SM because the only invisible particles of the SM are neutrinos. In this case, M_{T2} of the most background events, especially $t\bar{t}$ events, is lower than the top quark mass $m_{\rm top}$. This is because we can measure the parent particle mass with the correct test mass, and the top quark is the heaviest parent particle in the SM. Also, it was found that events without missing momentum or with fake missing momentum which is parallel to a mismeasured jet have very small values of M_{T2} [21]. If a significant excess of M_{T2} above $m_{\rm top}$ is observed, it should be the new physics signal.

On the other hand, M_{T2} of new physics is not bounded by the parent particle mass because the test mass is wrong for the Dark Matter candidate of new physics. The upper bound of M_{T2} is a mass combination of the parent particle and the invisible particle in the absence of USR,

$$M_{T2}^{\rm max} = \frac{m_{parent}^2 - m_{inv}^2}{m_{parent}} \equiv \mu_0. \tag{13}$$

In this case, the signal is extracted from the background for models with a large mass splitting, such as SUSY, but not for models with a degenerate mass spectrum, such as $\mu_0 \leq m_{\rm top}$, because the signal is buried in the background.

However, considering the recoil momentum of parent particles by USR, M_{T2} is still a useful variable for the event selection in searching for the nearly degenerate model: MUED. $M_{T2}^{\rm max}$ varies with USR and can exceed μ_0 due to the wrong test mass. For example, when parent particles of same mass are produced and directly decay to invisible particles emitting visible particles ($q^{(1)}q^{(1)} \to qq\gamma^{(1)}\gamma^{(1)}$), $M_{T2}^{\rm max}$ [38, 39] is

$$M_{T2}^{\rm max} = \sqrt{\mu(P_T)^2 + P_T\mu(P_T)} \geq \mu_0, \tag{14}$$

where

$$\begin{aligned} \mu(P_T) &\equiv \mu_0 \left(\sqrt{1 + \left(\frac{P_T}{2m_{parent}}\right)^2} - \frac{P_T}{2m_{parent}} \right) \\ &\to \mu_0 \left(\frac{m_{parent}}{P_T} \right) \qquad \text{for } P_T \gg m_{parent} \end{aligned} \tag{15}$$

where P_T is the magnitude of the momentum of USR. There is a rich source of USR because processes of heavy particles tend to come along with hard QCD radiations including ISR. Hard ISR gives large recoil of produced particles, and $M_{T2}^{\rm max}$ can have a large value depending on USR. Note that the background events do not have M_{T2} dependence on USR because the test mass is correct, so most events are kept lower than m_{top}.

When analyzing events, we cannot tell the origins of visible particles: whether the particles come from decays of heavier particles or are QCD radiations. Practically, leading two jets in p_T are used as visible particles to construct M_{T2}. If they correspond to two "correct" particles, namely if each particle is a decay product of each pair-produced particle, M_{T2} behaves as discussed above. However, the leading particles can be decay products of one parent particle, and also hard ISR can be one or both of the leading particles. These cases are called "combinatorics".

In many events, M_{T2} of the leading particles corresponds to M_{T2} of the correct particles. For instance, the rate of correspondence is about half for $q^{(1)}q^{(1)}$ or $t\bar{t}$ as shown later. Combinatorics smears the M_{T2} distribution. The smearing effect is significant for high M_{T2}, and it is different in each process.

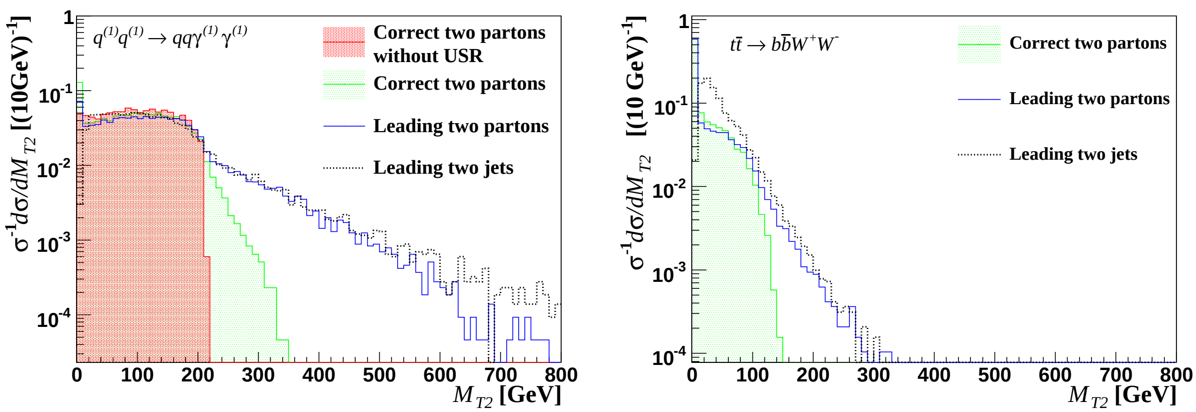

Figure 2: Distributions of M_{T2} for $q^{(1)}q^{(1)} \to qq\gamma^{(1)}\gamma^{(1)}$ in the left and $t\bar{t} \to b\bar{b}W^+W^-$ in the right generated by MadGraph/MadEvent 4.4 [40] where $m_{q^{(1)}} = 912.5$ GeV, $m_{\gamma^{(1)}} = 800.1$GeV, and $\mu_0 = 211.0$GeV. M_{T2} is constructed with the correct two partons (green shaded area), the leading two partons (blue solid line), and leading two jets (dotted line). Also, events were generated without additional jets, that is, without USR in the parton level, and M_{T2} was calculated with the correct two partons (red shaded area). The distributions are normalized to 1.

In order to see the effects of USR and combinatorics, we generated the $q^{(1)}q^{(1)}$ production of the MUED benchmark point and the $t\bar{t}$ production adding up to one jet in the parton level [2], and constructed M_{T2} with the correct partons and with the leading partons/jets. These

[2]The events were generated by MadGraph/MadEvent 4.4 at $\sqrt{s} = 14$ TeV. The fragmentation and

M_{T2} distributions are shown in fig. 2.

The green (red) shaded area shows M_{T2} with (without) an additional jet in the parton level using correct two partons: quarks from the direct decay $q^{(1)} \to q\gamma^{(1)}$ for $q^{(1)}q^{(1)}$ and b quarks from $t \to bW$ for $t\bar{t}$. LKPs and neutrinos produce $\mathbf{p}_T^{miss}$. For the signal, M_{T2} without USR (red shaded area) is bounded by the mass combination $\mu_0 = 210$ GeV given by (13). Including USR (green shaded area) M_{T2} varies with P_T and exceeds μ_0 as (14), and theoretically it reachs about 440 GeV with extremely large P_T. For the $t\bar{t}$ background, M_{T2} of correct two partons with USR (green shaded rarea) does not exceed m_{top} as expected.

Parton level	$q^{(1)}q^{(1)} \to qq\gamma^{(1)}\gamma^{(1)} + 0, 1$ jet	$t\bar{t} \to b\bar{b}W^+W^- + 0, 1$ jet
$M_{T2}^{leading} = M_{T2}^{correct}$	61.6%	49.1%
$M_{T2}^{leading} > M_{T2}^{correct}$	30.3%	22.4%
$M_{T2}^{leading} < M_{T2}^{correct}$	8.1%	28.5%

Table 2: The evaluation of combinatrics for $q^{(1)}q^{(1)}$ of the benchmark point and $t\bar{t}$. M_{T2} is constructed in the parton level. We compare M_{T2} of leading partons and correct partons in each event.

When the leading partons are used for M_{T2} (blue solid line), combinatorics smears the M_{T2} distribution. M_{T2} of the leading partons spreads over the endpoint of M_{T2} of correct partons to roughly double the value at the endpoint as in fig. 2. Table 2 shows the evaluation of combinatorics. The leading partons correspond to the correct partons for 60% of the time for $q^{(1)}q^{(1)}$ and for 50% for $t\bar{t}$. The smearing effect due to combinatorics is different in each process: $M_{T2}^{leading} > M_{T2}^{correct}$ for three quarters of the combinatorics events of $q^{(1)}q^{(1)}$, while $M_{T2}^{leading} < M_{T2}^{correct}$ for more than half of the combinatorics events of $t\bar{t}$. Therefore, combinatorics assists to enhance the signal to background ratio for high M_{T2}.

Also, the detector effects are simulated after the fragmentation and hadronization, and M_{T2} is constructed with the leading two jets (dotted line). The distribution is similar with the M_{T2} distribution with the leading two partons.

The dependence on USR makes the signal excess in the high M_{T2} region even for the nearly degenerate model, and the smearing effect of combinatorics enhances the excess. It can been seen that events with high M_{T2}, say above 200 GeV, are dominated by the $q^{(1)}q^{(1)}$ signal over the $t\bar{t}$ background. Since for the other SM background processes the parent particle is lighter than the top quark, those background events are expeced to have M_{T2} lower than m_{top}. Hence, M_{T2} is an effective event selection to search for the nearly degenerate model.

hadronization were simulated by PYTHIA 6.4, and the detector effects were simulated by PGS 4 [41]. The simulation setup is the same as the simulation described in Sec. 4 except that here only one jet was added as the Matrix Element correction. The MLM matching [42] was prescribed.

4 Simulation

4.1 Signal

Monte Carlo (MC) samples of MUED signal were generated both by a private implementation in MadGraph/MadEvent 4.4 (MG/ME) [40] and an implementation [43] in Pythia 6.4 [33]. CTEQ5.1L was used as the leading-order (LO) parton distribution function (PDF). In the case of MG/ME, the Matrix Element was calculated by HELAS [44], and the fragmentation and hadronization were simulated with Pythia. The effects of jet reconstruction and detector smearing were simulated through PGS 4 [41].

We consider $1/R$ from 400 GeV to 1.6 TeV in steps of 100 GeV with $\Lambda R = 10$, 20, 30, and 40. The remaining parameter, m_h, is set to 120 GeV. The MUED spectrum is simplified by neglecting m_{SM} for the first KK level. The processes we consider are pair productions of the colored first KK particles, $g^{(1)}$, $q^{(1)}$, and $Q^{(1)}$. The signal events corresponding to luminosities of 5 fb^{-1} at $\sqrt{s}$ = 7 TeV and of more than 10 fb^{-1} at $\sqrt{s}$ =14 TeV were generated by Pythia. Table 3 shows the production processes which can be generated in the Pythia implementation.

Process		flavor
KK gluon + KK gluon	$g + g \to g^{(1)} + g^{(1)}$	
KK quark + KK gluon	$g + q \to g^{(1)} + Q^{(1)};\ g^{(1)} + q^{(1)}$	
KK quark + KK quark	$q_i + q_j \to Q_i^{(1)} + Q_j^{(1)};\ q_i^{(1)} + q_j^{(1)}$	all i, j
	$q_i + q_j \to Q_i^{(1)} + q_j^{(1)}$	all i, j
KK quark + KK antiquark	$g + g \to Q^{(1)} + \bar{Q}^{(1)};\ q^{(1)} + \bar{q}^{(1)}$	
	$q + \bar{q} \to Q^{(1)} + \bar{Q}^{(1)};\ q^{(1)} + \bar{q}^{(1)}$	
	$q_i + \bar{q}_j \to Q_i^{(1)} + \bar{q}_j^{(1)}$	$i \neq j$
	$q_i + \bar{q}_j \to Q_i^{(1)} + \bar{Q}_j^{(1)};\ q_i^{(1)} + \bar{q}_j^{(1)}$	$i \neq j$
	$q_i + \bar{q}_i \to Q_j^{(1)} + \bar{Q}_j^{(1)}$	$i \neq j$

Table 3: Processes of MUED generated by the Pythia implementation [43]. $SU(2)_L$ doublet and singlet first KK quark are denoted by $Q^{(1)}$ and $q^{(1)}$ respectively.

Since we use the M_{T2} dependence on USR, the ISR has an important role. In order to reliably evaluate the hard ISR, we considered the Matrix Element correction in MG/ME adding up to one jet to the pair productions. The MLM matching [42] was applied to remove the overlap between jets from the Matrix Element and ones from the Parton Shower. This prescription was demonstrated for the benchmark point of $\Lambda R = 20$ and $1/R = 800$ GeV. The spectrum of this point is listed in table 1. However it is very time consuming to generate all of the signal MC samples with the Matrix Element correction, so we used PYTHIA rather than MG/ME to generate them for the discovery study. We will show in Sec. 5.2. that MC samples generated by ME/ME with the Matrix Element correction have larger excess over background than ones generated by PYTHIA for the benchmark point. Hence, the event generation by PYTHIA is conservative.

4.2 Background

MC samples of the SM background, $t\bar{t}$, $W/Z+jets$, Diboson ($WW, WZ,$ and ZZ), etc., were produced with MG/ME using the PDF set CTEQ6.1L, and fragmentation and hadronization were simulated with PYTHIA in the same way of the signal. For $t\bar{t}$, $W/Z+jets$, and Diboson, up to two partons were added in the Matrix Element and the MLM matching was prescribed. The MC samples were detector-simulated through PGS 4. The dominant background processes, $t\bar{t}$ and $W/Z+jets$, were normalized to the next-leading-order (NLO) cross section consistent with the inclusive dijet analysis of the ATLAS MC study [45].

For the sake of comparison with the $4l + E_T^{miss}$ analysis, we generated some multilepton background processes, such as four leptons through off-shell Z^* or γ^*. The luminosities of generated SM background are more than 2 fb^{-1} at $\sqrt{s}$= 7 and more than 10 fb^{-1} at $\sqrt{s}$= 14 TeV, respectively. The summary of the background processes is shown in table 4.

Process	$\sqrt{s} = 7$ TeV $\boldsymbol{\sigma}\times$ efficiency	$\sqrt{s} = 14$ TeV $\boldsymbol{\sigma}\times$ efficiency
$t\bar{t} + 0, 1, 2$ jets	130 pb	765 pb
$(W \to l\nu) + 1, 2$ jets†	287 pb	897 pb
$(Z \to l^+l^-, \nu\bar{\nu}) + 1, 2$ jets†	98.8 pb	341 pb
$W^+W^- + 0, 1, 2$ jets	35.0 pb	97.5 pb
$WZ + 0, 1, 2$ jets	15.0 pb	44.1 pb
ZZ +0, 1, 2 jets	4.78 pb	12.9 pb
$Z^*/\gamma^* Z^*/\gamma^* \to 2l^+2l^-$	29.2 fb	57.2 fb
$Z + b\bar{b}$	35.5 pb	135 pb
$W + b\bar{b}$	22.5 pb	55.0 pb
$(Z/\gamma^* \to l^+l^-, \nu\bar{\nu}) + t\bar{t}$	28.7 fb	205 fb
$(W \to l\nu) + t\bar{t}$	37.2 fb	131 fb

Table 4: Summary of the SM datasets used in this analysis. +n jets are added in Matrix Elements with the MLM matching. †MC samples of $W/Z + jets$ are preselected as $p_T^{\rm 1stjet} >$ 90 GeV. The cross sections listed are calculated with the preselected MC samples generated by MADGRAPH/MADEVENT 4.4.

5 Analysis

5.1 Object selection

The object selection is that an electron and a muon are required to have $p_T > 10$ GeV and $|\eta| < 2.5$ and a jet is required to have $p_T > 20$ GeV and $|\eta| < 2.5$. In order to avoid recognizing a shower from an electron as a jet, a jet within $\Delta R < 0.2$ ($\Delta R = \sqrt{\Delta\eta^2 + \Delta\phi^2}$) from any electron is removed. Charged leptons from hadronic activity also should be removed. If an electron and a jet are found within $0.2 < \Delta R < 0.4$, the jet is kept and the electron is rejected Similarly, if a muon and a jet are found within $\Delta R < 0.4$, the muon is rejected.

5.2 Event selection

First, we require two jets with $p_T^{jet} > \{100,\ 20\ \text{GeV}\}$, and p_T^{miss} (E_T^{miss}) must exceed 100 GeV. Cuts stronger than these will reduce the MUED signal. At least one charged lepton, an electron or a muon, with $p_T^{lep} > 20$ GeV is required in our analysis. The cuts imposed above, particularly the requirement of one lepton, are necessary to avoid the QCD background. Either $\{p_T^{jet1} > 100\ \text{GeV}, p_T^{miss} > 100\ \text{GeV}\}$ or $p_T^{lep} > 20$ GeV is used as a trigger. When there is only one lepton, we impose a cut of $M_T^{lep,miss} > 100$ GeV to reduce the $W + jets$ background, where

$$M_T^{lep,miss} \equiv \sqrt{2\left(p_T^{lep} p_T^{miss} - \mathbf{p}_T^{lep} \cdot \mathbf{p}_T^{miss}\right)} \quad .$$

Finally, we construct M_{T2} with the leading two jets, and impose $M_{T2} > 200$ GeV. To summarize our event selection:

- CUT1: $p_T^{jet} > \{100, 20\ \text{GeV}\}$
- CUT2: $E_T^{miss} > 100$ GeV
- CUT3: At least one lepton with $p_T^{lep} > 20$ GeV
- CUT4: If the number of lepton is one, $M_T^{lep,miss} > 100$ GeV
- CUT5: $M_{T2} > 200$ GeV.

In order to demonstrate the effectiveness of M_{T2} for the MUED, we only use the basic cuts 1-4 except one on M_{T2}. The cuts 1-4 are comparable with ones imposed in the ATLAS and CMS new physics searches in one lepton + jets + E_T^{miss} with low luminosity at $\sqrt{s} = 7$ TeV [46, 47]. We do not use the M_{eff} cut and the E_T^{miss}/M_{eff} cut which are used to extract the signal especially by the ATLAS collaboration in the search for SUSY [45], where

$$M_{eff} \equiv \sum_{jet}^{4} p_T + \sum_{lepton} p_T + E_T^{miss}. \tag{16}$$

It is common that the $\Delta\phi_{jet,miss}$ cut is applied to reduce events with fake missing due to the mismeasurement of jets, but this is not necessary because the later M_{T2} cut has a similar role [21].

Process		CUT1	CUT2	CUT3	CUT4	CUT5 (Optimal)
$g^{(1)} + g^{(1)}$	MG/ME	1,028	832	119	62	25
	PYTHIA	937	757	108	63	22
$g^{(1)} + q^{(1)}/Q^{(1)}$	MG/ME	9,196	7,218	1,234	675	241
	PYTHIA	8,569	6,694	1,344	731	223
$q^{(1)}/Q^{(1)}$ $+q^{(1)}/Q^{(1)}$	MG/ME	5,315	4,035	863	508	148
	PYTHIA	4,497	3,276	690	436	84
$q^{(1)}/Q^{(1)}$ $+\bar{q}^{(1)}/\bar{Q}^{(1)}$	MG/ME	1,444	1,075	206	115	27
	PYTHIA	1,301	955	163	112	20
Total MUED	MG/ME	16,983	13,160	2,422	1,360	441
	PYTHIA	15,304	11,682	2,305	1,342	349
$t\bar{t}$		426,074	57,533	23,239	5,620	243
W		400,527	97,907	35,386	1,031	85
Z		142,368	53,801	916	107	12
$W/Z + t\bar{t}/b\bar{b}$		1,121	304	103	49	10
Diboson		29,141	4,482	1,335	252	40
Total Standard Model		999,231	214,027	60,979	7,059	390
Total MUED Z_B	MG/ME	0.05	0.17	0.06	0.78	4.10
	PYTHIA	0.05	0.14	0.05	0.77	3.37 (7.57)

Table 5: Cut flow for 1 fb^{-1} at $\sqrt{s} = 14$TeV. The MUED benchmark point is $\{1/R, \Lambda R\} = \{800 \text{ GeV}, 20\}$. The MUED signal generated by MadGraph/MadEvent 4.4 (MG/ME) with the MLM matching is normalized to one generated by Pythia. $M_{T2} > 350$ GeV is an optimal cut that maximizes the significance $Z_B = 7.57$.

The cut flow in table 5 shows that the M_{T2} cut (CUT5) significantly reduces the SM background to a level comparable to the MUED. Since the Matrix Element correction increases event rates in the high M_{T2} region, there remain more signal events generated by MG/ME after CUT5 than ones generated by Pythia. Therefore, the signal rate in the fast event generation by Pythia is a little underestimated and hence is conservative.

Fig. 3 shows that the dominant background are $t\bar{t}$, $W + jets$, and Diboson. Background events that remain even after CUT5 mainly come from combinatorics. The peak of MUED events is $M_{T2} < 200$ GeV, but the signal events have a long tail which can be understood as a result of the variant endpoint due to the wrong test mass discussed in section 3.2. There is combinatorics for both the signal and the background, and especially it tends to increase M_{T2} of the signal events. Combinatorics help to enhance the signal excess. As a result, we can successfully extract the signal from the background even based on jets.

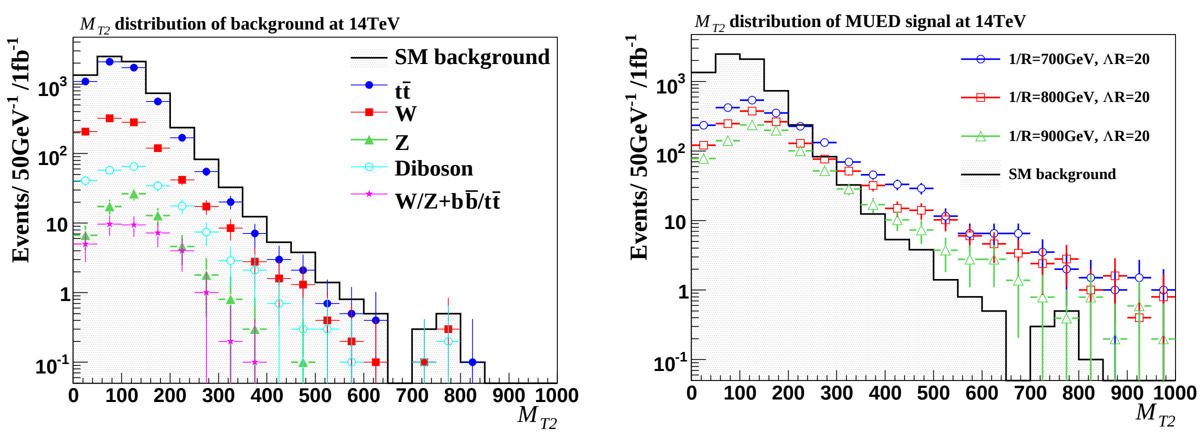

Figure 3: Distributions of M_{T2} of the leading two jets after CUT4 for each SM background in the left, and total SM background and MUED signal points of $1/R = 700, 800, 900$ GeV and $\Lambda R = 20$ generated by PYTHIA in the right.

5.3 Discovery potential

For the study of the discovery potential it is necessary to take systematic uncertainties into account in addition to statistical uncertainties. We use the significance Z_B [48], which is provided by the ROOT library [49], using the same approach as in the ATLAS discovery study of the SUSY [45]. Z_B is calculated using a convolution of a Poisson and a Gaussian term to account for systematic errors. For the backgrounds except those from QCD, a reasonable estimate of the systematic uncertainty is $\pm 20\%$. The discovery potential is studied by finding the optimal M_{T2} cut (in step of 50GeV) to maximize the significance Z_B. We define "discovery" when $Z_B > 5$ and more than 10 signal events remain after the cuts.

In order to compare the M_{T2} analysis in the multijet + lepton mode with the previously studied $4l + E_T^{miss}$ analysis, we also check the discovery potential in $4l + E_T^{miss}$ using the same MC samples and using the same definition of discovery. In the $4l + E_T^{miss}$ analysis, the following cuts are imposed [14]:(1) four isolated leptons with $p_T^{lep} > \{35, 20, 15, 10 \text{ GeV}\}$ are required, (2) $E_T^{miss} > 50$ GeV, and (3) an invariant mass M_{ll} for all possible pairs of opposite sign same flavor leptons and remove events if $|M_{ll} - m_Z| < 10$ GeV to reduce background from the Z boson. The estimated background from our MC samples is 10 events/100 fb^{-1}. The fake leptons should be considered to evaluate the background level of $4l + E_T^{miss}$ more appropriately, but the fake leptons are not considered since they are not important for our analysis based on jets.

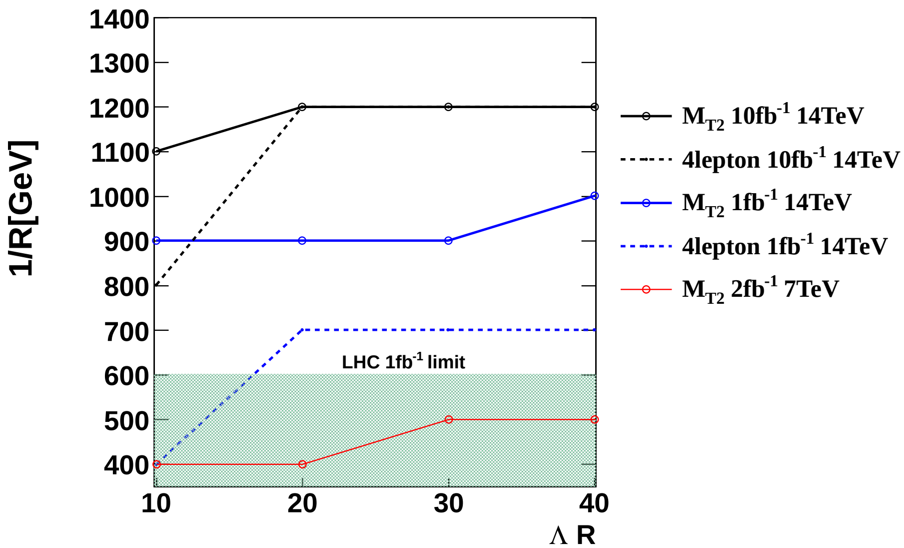

Figure 4: Discovery potential of the MUED with 1 fb^{-1} and 10 fb^{-1} at $\sqrt{s} = 14$ TeV in the $4l + E_T^{miss}$ analysis and the M_{T2} analysis and discovery potential of 2 fb^{-1} at $\sqrt{s} = 7$ TeV only in the M_{T2} analysis. For a given luminosity, the parameter region below the line will be discovered.

The spectrum is more degenerate for smaller ΛR, which is more difficult for discovery in general. Note that for fixed $1/R$, the MUED with smaller ΛR has a larger cross section simply because the KK gluon and the KK quark become lighter as in Eqs. (7) and (8). Fig. 4 shows that the discovery potential does not vary with changing ΛR in the M_{T2} analysis. The first run of LHC at $\sqrt{s} = 7$ TeV will have an integrated luminosity of 2 fb^{-1} and so it can discover up to $1/R \sim 500$ GeV. However this parameter region was already excluded by the ATLAS multijet+E_T^{miss} analysis with 1 fb^{-1}, as mentioned in Sec. 2.4. The second run at 14 TeV will discover up to $1/R \sim 1$ TeV with 1 fb^{-1} and $1/R \sim 1.2$ TeV with 10 fb^{-1}.

In the $4l + E_T^{miss}$ analysis, the discovery reach at 14 TeV is $1/R \sim 700$ GeV with 1 fb^{-1} and $1/R \sim 1.2$ TeV with 10 fb^{-1} for $20 \leq \Lambda R \leq 40$, but the sensitivity is very low for $\Lambda R = 10$: the discovery reach is only $1/R = 400$ GeV with 1 fb^{-1} and $1/R = 800$ GeV with 10 fb^{-1}.

The result shows that our M_{T2} analysis improves the discovery potential. In particular, the improvement is so significant for the most degenerate parameter $\Lambda R = 10$ that the discovery potential improves from $1/R = 400$ GeV to 900 GeV.

6 Discussion and Conclusion

We have improved the discovery potential of the MUED. We include the background systematic uncertainties. The previously studied multilepton channels, such as $4l + E_T^{miss}$, are clean channels but only sensitive to the limited number of processes. On the other hand, we utilize the multijet + lepton channel, and it is accessible to the most processes of the MUED. Although this channel is statistically advantageous, it difficult to extract the MUED signal events from backgrounds. However, we succeeded in extracting the signal from the background by applying M_{T2} for the event selection. This is because the signal events can have large values of M_{T2} thanks for the dependence on USR with the wrong test mass, and because the combinatorics effect enhances the signal excess.

The simulation result indicates that the discovery potential is significantly improved by using M_{T2} cut. The most important achievement is that our M_{T2} analysis has a much greater sensitivity for the MUED for the most degenerate mass spectrum than the $4l+E_T^{miss}$ analysis. For 1 fb^{-1} at $\sqrt{s} = 14$ TeV, the discovery potential increases by 500 GeV in terms of $1/R$ for the fixed $\Lambda R = 10$. Therefore, the M_{T2} analysis is particularly effective for the case of a highly degenerate spectrum.

The relic abundance of the Dark Matter implies that the very high value of $1/R \sim 1.5$ TeV is favored, while our analysis reaches only up to $1/R \sim 1.2$ TeV with 10 fb^{-1} at $\sqrt{s} = 14$ TeV. However, there is possibility to improve the discovery potential further. We considered the Matrix Element correction and the NLO correction to the background. If those corrections to the signal are included, the Matrix Element correction enhances the event rate for high M_{T2} as shown in Sec. 5.2, and the NLO correction increases the cross section. Also, additional cuts, such as the b-jet veto and E_T^{miss}/M_{eff}, could enlarge the discovery potential of the MUED, although we did not introduce them in order to emphasize the effectiveness of M_{T2}. The b-jet veto must be particularly effective because it significantly reduces the $t\bar{t}$ background. Including these effects the discovery reach will be improved, and the Dark Matter favored MUED may be searched with $O(100)$ fb^{-1}.

The search using M_{T2} has a model independent aspect. The benefit of the M_{T2} analysis is significant when there is large USR. We might expect large USR because a common feature of many new physics models is production of heavy colored particles associated with hard ISR contained in USR. This analysis is also applicable to other models: SUSY with R parity or Little Higgs model with T parity with a nearly degenerate mass spectrum.

For our analysis, we required one lepton to avoid the QCD background, but this is not always necessary. If the well-understood QCD MC samples are prepared, we can study the discovery potential based on the M_{T2} analysis in the inclusive dijet channel, which is statistically advantageous and is accessible to models that rarely emit leptons.

Because of the significant improvement of the search for MUED by using M_{T2}, this work implies that the LHC will be able to have better sensitivities to nearly degenerate models. A more general analysis with a nearly degenerate spectrum is left to a future work.

Acknowledgement

We thank Shoji Asai, Shigeki Matsumoto, Seong Chang Park, Ryosuke Sato and Satoshi Shirai for useful discussions. This work is supported by the World Premier International Research Center Initiative (WPI initiative) MEXT, Japan. H.M. was supported in part by the U.S. DOE under Contract DE-AC03-76SF00098, in part by the NSF under grant PHY-04-57315, and in part by the Grant in-Aid for scientic research (23540289) from Japan Society for Promotion of Science (JSPS). M. N. was also supported by the Grant-in-Aid for scientific research (22540300) from JSPS.

References

[1] T. Appelquist, H.-C. Cheng, and B. A. Dobrescu, Phys. Rev. **D64** (2001) 035002, [hep-ph/0012100].

[2] D. Hooper and S. Profumo, Phys.Rept. **453** (2007) 29–115, [hep-ph/0701197].

[3] N. Arkani-Hamed, S. Dimopoulos, and G. R. Dvali, Phys. Lett. **B429** (1998) 263–272, [hep-ph/9803315].

[4] L. Randall and R. Sundrum, Phys. Rev. Lett. **83** (1999) 3370–3373, [hep-ph/9905221].

[5] G. Servant and T. M. P. Tait, Nucl. Phys. **B650** (2003) 391–419, [hep-ph/0206071].

[6] H.-C. Cheng, K. T. Matchev, and M. Schmaltz, Phys. Rev. **D66** (2002) 036005, [hep-ph/0204342].

[7] H. Georgi, A. K. Grant, and G. Hailu, Phys. Lett. **B506** (2001) 207–214, [hep-ph/0012379].

[8] K. Kong and K. T. Matchev, JHEP **0601** (2006) 038, [hep-ph/0509119].

[9] F. Burnell and G. D. Kribs, Phys.Rev. **D73** (2006) 015001, [hep-ph/0509118].

[10] M. Kakizaki, S. Matsumoto, Y. Sato, and M. Senami, Nucl. Phys. **B735** (2006) 84–95, [hep-ph/0508283].

[11] M. Kakizaki, S. Matsumoto, Y. Sato, and M. Senami, Phys. Rev. **D71** (2005) 123522, [hep-ph/0502059].

[12] G. Belanger, M. Kakizaki, and A. Pukhov, JCAP **02** (2011) 009, [hep-ph/1012.2577].

[13] K. Kawagoe and M. M. Nojiri, Phys. Rev. **D74** (2006) 115011, [hep-ph/0606104].

[14] H.-C. Cheng, K. T. Matchev, and M. Schmaltz, Phys. Rev. **D66** (2002) 056006, [hep-ph/0205314].

[15] C. Macesanu, C. D. McMullen, and S. Nandi, Phys.Rev. **D66** (2002) 015009, [hep-ph/0201300].

[16] M. Kazana, Acta Phys. Polon. **B38** (2007) 449–458, [CERN-CMS-CR-2006-062].

[17] G. Bhattacharyya, A. Datta, S. K. Majee, and A. Raychaudhuri, Nucl.Phys. **B821** (2009) 48–64, [hep-ph/0904.0937].

[18] B. Bhattacherjee and K. Ghosh, Phys. Rev. **D83** (2011) 034003, [hep-ph/1006.3043].

[19] C. Lester and D. Summers, Phys.Lett. **B463** (1999) 99–103, [hep-ph/9906349].

[20] A. Barr, C. Lester, and P. Stephens, J.Phys.G **G29** (2003) 2343–2363, [hep-ph/0304226].

[21] A. J. Barr and C. Gwenlan, Phys. Rev. **D80** (2009) 074007, [hep-ph/0907.2713].

[22] C. Lester and A. Barr, JHEP **0712** (2007) 102, [hep-ph/0708.1028].

[23] **ATLAS** Collaboration, J. B. G. da Costa *et al.*, [hep-ex/1102.5290].

[24] **CMS** Collaboration, CMS-PAS-SUS-11-005.

[25] G. Bhattacharyya, A. Datta, S. K. Majee, and A. Raychaudhuri, Nucl. Phys. **B760** (2007) 117–127, [hep-ph/0608208].

[26] I. Gogoladze and C. Macesanu, Phys. Rev. **D74** (2006) 093012, [hep-ph/0605207].

[27] T. Appelquist and H.-U. Yee, Phys.Rev. **D67** (2003) 055002, [hep-ph/0211023].

[28] K. Agashe, N. Deshpande, and G. Wu, Phys.Lett. **B514** (2001) 309–314, [hep-ph/0105084].

[29] A. J. Buras, A. Poschenrieder, M. Spranger, and A. Weiler, Nucl. Phys. **B678** (2004) 455–490, [hep-ph/0306158].

[30] U. Haisch and A. Weiler, Phys. Rev. **D76** (2007) 034014, [hep-ph/0703064].

[31] **ATLAS** Collaboration, G. Aad *et al.*, [hep-ex/1109.6572].

[32] **ATLAS** Collaboration, [hep-ex/1109.6606].

[33] T. Sjostrand, S. Mrenna, and P. Z. Skands, JHEP **05** (2006) 026, [hep-ph/0603175].

[34] W. S. Cho, K. Choi, Y. G. Kim, and C. B. Park, Phys. Rev. Lett. **100** (2008) 171801, [hep-ph/0709.0288].

[35] A. J. Barr, B. Gripaios, and C. G. Lester, JHEP **02** (2008) 014, [hep-ph/0711.4008].

[36] W. S. Cho, K. Choi, Y. G. Kim, and C. B. Park, JHEP **02** (2008) 035, [hep-ph/0711.4526].

[37] M. M. Nojiri, Y. Shimizu, S. Okada, and K. Kawagoe, JHEP **06** (2008) 035, [hep-ph/0802.2412].

[38] M. Burns, K. Kong, K. T. Matchev, and M. Park, JHEP **03** (2009) 143, [hep-ph/0810.5576].

[39] T. Cohen, E. Kuflik, and K. M. Zurek, JHEP **11** (2010) 008, [hep-ph/1003.2204].

[40] J. Alwall *et al.*, JHEP **09** (2007) 028, [hep-ph/0706.2334].

[41] J. Conway, http://www.physics.ucdavis.edu/conway/research/software/pgs/pgs4-general.htm.

[42] J. Alwall *et al.*, Eur. Phys. J. **C53** (2008) 473–500, [hep-ph/0706.2569].

[43] M. ElKacimi, D. Goujdami, H. Przysiezniak, and P. Z. Skands, Comput. Phys. Commun. **181** (2010) 122–127, [hep-ph/0901.4087].

[44] H. Murayama, I. Watanabe, and K. Hagiwara.

[45] **ATLAS** Collaboration, G. Aad *et al.*, [hep-ex/0901.0512].

[46] **CMS** Collaboration, C. Bernet, [hep-ex/1105.5911].

[47] **ATLAS** Collaboration, G. Aad *et al.*, Phys.Rev.Lett. **106** (2011) 131802, [hep-ex/1102.2357].

[48] J. T. Linnemann, [physics/0312059].

[49] R. Brun and F. Rademakers, Nucl.Instrum.Meth. **A389** (1997) 81–86.